Nanoscale

Accepted Manuscript

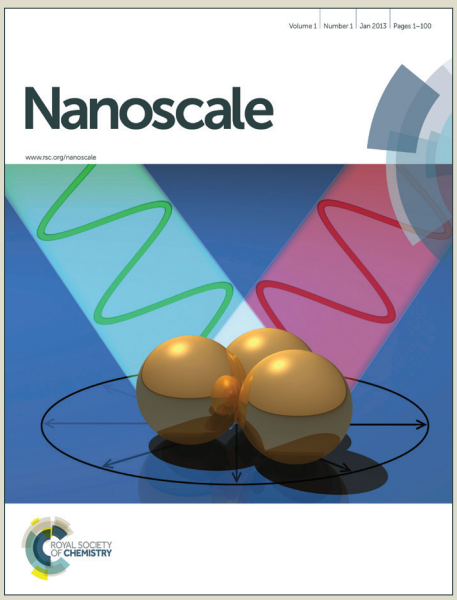

ROYAL SOCIETY OF CHEMISTRY

www.rsc.org/nanoscale

Cite this: DOI: 10.1039/c0xx00000x

www.rsc.org/xxxxxx

ARTICLE TYPE

High-performance humidity sensors from $Ni(SO_4)_{0.3}(OH)_{1.4}$ nanobelts

Ming Zhuo[1], Yuejiao Chen[1], Tao Fu[2], Haonan Zhang[1], Zhi Xu[2], Qiuhong Li*[a1] and Taihong Wang*[b1]

Received (in XXX, XXX) Xth XXXXXXXXX 20XX, Accepted Xth XXXXXXXXX 20XX
DOI: 10.1039/b000000x

$Ni(SO_4)_{0.3}(OH)_{1.4}$ nanobelts were synthesized by a facile hydrothermal method. Humidity sensors based on $Ni(SO_4)_{0.3}(OH)_{1.4}$ nanobelts were fabricated and exhibited high sensitivity and fast response. It also showed good long-term stability. The high performance could be related to the high surface to volume ratio of nanobelts and the chemical composition of $Ni(SO_4)_{0.3}(OH)_{1.4}$.

Humidity displays an extensive influence on human comfort, industry manufacturing and packaging, medical care, meteorological forecast and so on.[1-5] There is a substantial interest in the development of sensors for application in monitoring and detecting humidities in moisture-sensitive environment, such as glove boxes and clean rooms.

It has shown that nanomaterial-based devices have great potential for humidity sensors. Various methods have been developed.[6-10] One dimensional (1D) nanomaterials offer a promising platform for high-performance sensing devices that employ favourable electronic transport. With large surface to volume ratio, they are expected to behave high performance because of more active sites available on the surface of the material for physical or chemical interaction.[11-13] Many humidity sensors based on 1D nanomaterials have been reported.[14-18] But it is still a big challenge for the realization of sensors with high sensitivity, fast response, long-term stability, low cost and facile fabrication technique. Novel materials are being explored.[19]

Nickel hydroxide has attracted great interest as cathode material in alkaline batteries.[20-23] Being intercalated with anions or water molecules, it will form hydroxyl-rich nickel basic salts, having a composition of $-Ni(A^{n-})_{x/n}(OH)_{2-x}{\cdot}yH_2O$ (where x=0.5~1, A=NO^{3-}, Cl^-, SO_4^{2-}).[24-25] Nanostructures of these salts have been realized. $Ni(SO_4)_{0.3}(OH)_{1.4}$, as a typical compound with 1D structure, has been reported by several groups, in which the synthesis methods and its electrochemical properties are investigated.[26-29] However, there are few reports to explore its sensing properties. In this work, $Ni(SO_4)_{0.3}(OH)_{1.4}$ nanobelts (NSOH NBs) with uniform morphology were synthesized on a large scale using a facile hydrothermal method. The sensors were fabricated using the NSOH NBs as sensitive material. Electrical characteristics and humidity sensing properties were investigated, which showed high sensitivity, good long-term stability and fast response.

The $Ni(SO_4)_{0.3}(OH)_{1.4}$ nanobelts were synthesized in 25 mL de-ionized water, together with 2.0 mmol nickel acetate and 2.0 mmol sodium sulfate at 150 °C for 20 h. The morphology of the samples was examined by scanning electron microscope (SEM) with Hitachi-4800. Fig. 1a shows the typical SEM image which indicates the product consists of large quantity of nanobelts with the length about 10 to 20 μm. The phase purity and crystal structure of the nanobelts was characterized by X-ray Diffraction (XRD) on a JEOL X-ray diffractomer using Cu-kα radiation at 40 kV and 250 mA, as shown in Fig. 1b. Obviously, all the diffraction peaks can correspond well to standard card of monoclinic paraotwayite (JCPDS No: 41-1424). No peaks of impurities or other phases were detected. The XRD pattern of the sample after kept in air for one year is given in Fig. S1. It shows little change. Further details were carried out by transmission electron microscope (TEM) with JEOL JEM-3010. The TEM specimen was prepared by placing a drop of the nanobelts dispersed in ethanol on a Cu grid covered with a holey carbon film. Fig. 1c reveals the belt-like morphology, according with SEM images. A high-resolution TEM (HRTEM) image is observed in Fig. 1d, which displays an obvious crystalline lattice with interplane spacing of 0.2208 nm, corresponding to the (10-6) plane of NSOH phase. The selected-area electron diffraction (SAED) pattern (Fig. S2) reveals the single crystal nature of the obtained material.

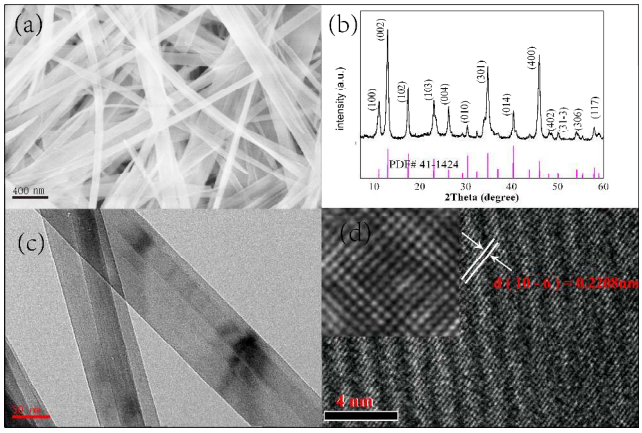

Fig. 1 (a) SEM images (b) XRD pattern of the $Ni(SO_4)_{0.3}(OH)_{1.4}$ nanobelts. (c) TEM and (d) HRTEM images of the $Ni(SO_4)_{0.3}(OH)_{1.4}$ nanobelts. The inset in (d) is the enlarged part of (d).

Humidity sensors based on $Ni(SO_4)_{0.3}(OH)_{1.4}$ nanobelts were fabricated by a simple drop method on interdigital gold electrodes on ceramic substrate. The width and length of the

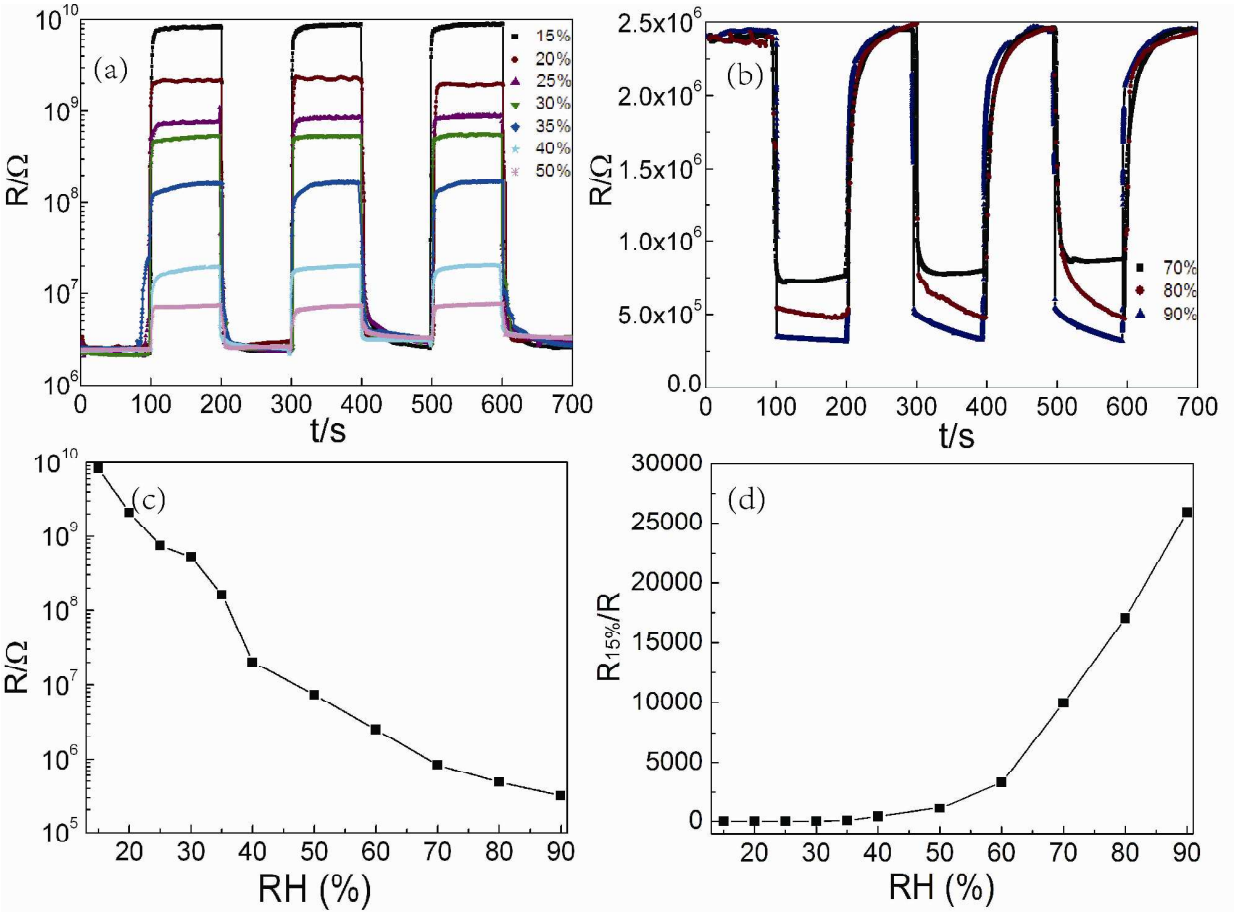

Fig. 2 (a, b) Real-time response of the RH sensor under different RHs. (c) Resistance of the sensor under each RH. (d) The ratio under different RH. The red line is the exponential fitting between the ratio and RH.

interdigital electrode are about 2.8 and 3.5 mm, respectively. The strip width of each finger is about 90 μm and the distance between each strip electrode is about 70 μm. For preparation, the ceramic substrate was cleaned by diluted HCl, acetone and de-ionized water respectively. The as-synthesized NSOH NBs were mixed with ethanol by ultrasonic for 1 h. After that, a drop of the suspension was coated on the substrate. The device was heated at 60 °C for the volatilization of ethanol. Bare Au interdigital electrodes and electrodes with sensing material are shown in the inset of Fig. S2. The sensing material formed thin film in light-green color. The corresponding current-voltage (*I-V*) curve was obtained by an Agilent 4156C precision semiconductor parameters analyzer, as shown in Fig. S3. The *I-V* curve was measured in the air ambient.

The humidity sensing properties were measured by using a high precision sensor testing system NS-4003 series (China Zhong-Ke Micro-nano IOT Ltd). Temperatures and humidities were precisely controlled through a climate test chamber C 180-40 (Weiss-voetsch Environmental Testing instruments, Tai Cang Co., Ltd). The chamber volume is 190 L. A schematic illustration of the sensor test system is shown in Fig. S4. The relative humidity (RH) and temperature of the atmosphere were 60% and 20 °C, respectively.

The resistance as a function of RH in aspect of time of the sensor was tested by NS-4003 series with an applied DC voltage of 5 V. The resistance variation as a function of RH at a constant temperature of 20 ℃ is presented in Fig. 2. Fig. 2a is the real-time resistance response between ambient air (60%) and different lower RH (15%, 20%, 25%, 30%, 35%, 40%, 50%) at 20 ℃. It indicates a strong influence of humidity on the resistance of the sensor which increases with decreasing RH. Under 60% RH, the resistance ($R_{60\%}$) is about 2.5×10^6 Ω, which quickly increases and rapidly reaches 8.32×10^9 Ω when the sensor is put in the chamber of 15% RH. After the RH is back to 60%, the resistance abruptly decreases and then gradually returns to original 2.5×10^6 Ω. The corresponding response time and recovery time (defined as the time required to reach 90% of the final equilibrium value) are about 3 s. In Fig. 2b, the measurement is based on dynamic switches of the sensor between ambient air (60%) and relatively higher RH. After exposed to 70%, 80%, and 90% RH, the sensor displays corresponding resistance of about 7.94×10^5, 4.88×10^5, and 3.21×10^5 Ω, respectively. The response and recovery time is longer than that when RH changes from 60% to lower humidities, which is obvious to observe in the latter two cycles shown in Fig. 2(b). The resistance (log (Ω)) as a function of RH is given in Fig. 2c, which shows that the resistance of the film decreases monotonically with increasing RH in the test range of 15% — 90%. Obviously, the resistance of the film changes by more than four orders of magnitude (from 10^5 Ω to nearly 10^{10} Ω), showing ultra-high sensitivity compared with many metal oxide humidity sensors.[6, 30-32] The ratio *S* is defined as $R_{15\%}/R$, and *R* is the resistance under higher RH, that is, 20%, 25%, 30%, 35%, 40%, 50%, 60%,

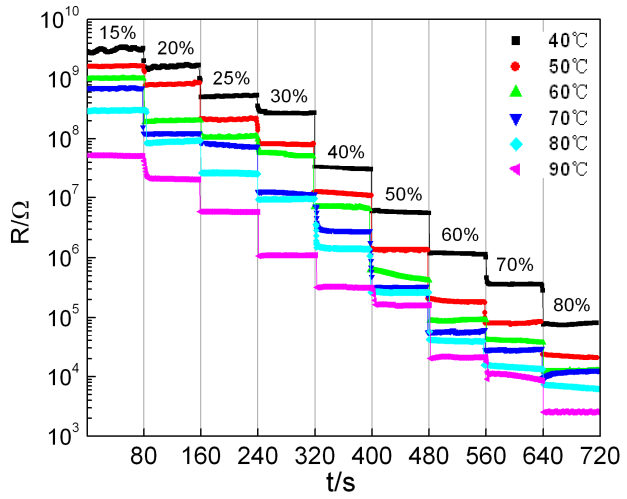

Fig. 3 The resistance decreases with RH at different temperatures.

70%, 80%, and 90% RH. The result is shown in Fig. 2d. *S* increases largely with RH. From 15% to 30%, it linearly increases with slope 1. From 35% to 50%, *S* linearly increases with slope 71.7. From 60% to 90%, *S* linearly increases with slope 753. The performance of the sensor in dry air was also measured. The resistance R_{dry} is 3.14×10^{10} Ω. Its corresponding sensitivity is given in Fig. S5.

To check its humidity sensitive characteristics of the sensor under different temperatures, resistance variations as a function of time were shown in Fig. 3. The measurements were carried out by RH changing from 15%, 20%, 25%, 30%, 40%, 50%, 60%, 70% to 80% when the temperature was controlled to be 40, 50, 60, 70, 80, 90 ℃, respectively. The sensor resistance decreases with RH, consistent with the result before. The result shows that the sensor exhibits similar properties under different temperatures.

The long-term stability is an important parameter for the practical applications of humidity sensor. Herein, the stability of the NSOH NBs sensor was monitored under different humidity conditions for 3 months. Fig. 4 shows the real-time resistance response of the sensor with different RHs at 20 ℃ after 3 months. It can be observed that the resistance just varies slightly less than 5% over the entire humidity region,

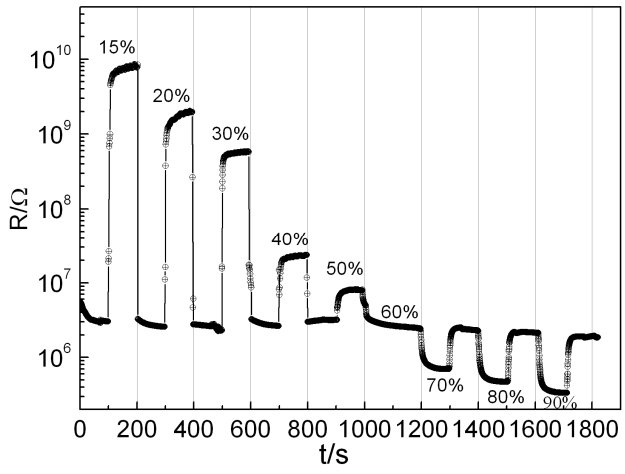

Fig. 4 The real-time resistance response with different RHs after 3 months.

indicating the NSOH NBs sensor displays excellent long-term stability.

The good sensing ability of the $Ni(SO_4)_{0.3}(OH)_{1.4}$ nanobelts sensor to humidity probably can be attributed to its structure and OH^-, SO_4^{2-} groups of $Ni(SO_4)_{0.3}(OH)_{1.4}$ nanobelts. Literatures have shown that 1D nanomaterial with high specific surface is highly advantageous for gas sensing, as it has a large exposure of surface atoms providing more active sites for the adsorption of gas sensing reaction, as it has a large exposure of surface atoms providing more active sites for the adsorption of gas molecules and hence promoting the surface reactions.[14-15, 30]

Humidity sensing is related to water adsorption and desorption process.[33-35] According to J. H. Anderson et al., protons could act as charge carriers during humidity sensing process.[36] At low humidity, tips and defects of the nanomaterial present a high local charge density and a strong electrostatic field, which promotes water dissociation.[33] The dissociation provides protons and hydroxyl groups. Protons hop along the nanobelt, contributing to the conductance. Water molecule layer is then physisorbed on the hydroxyl groups. At higher humidity, further physisorbed water layers are adsorbed on the first water layer. H_3O^+ appears and serves as a charge carrier.[37-40] In our work, OH^- groups exists initially in NSOH NBs. It could be effective sites to adsorb water molecules, which is believed to be a great contribution for NSOH NBs to exhibit a better performance. Fig. S7a shows nanobelt without the chemical composition OH^-. The OH^- shown in Fig. S5a is formed by dissociation of water and then absorbed on the surface of the nanobelts. While the nanobelt contains OH^- as shown in Fig. S7b, the water dissociation also happens. In the same time, it has more active sites to adsorb water molecules, thus more protons take part in the conduction, leading to the decrease of the resistance. When humidity gets even higher, more water molecules layers are adsorbed on the humidity sensor. Liquid water layers form on the surface of the nanobelt. In experimental section, *S* increases with humidity, with different slope in three RH regions. The response/recovery time also increase when RH changes from 60% to higher humidites. These experimental results could be related to the three humidity sensing process.

In conclusion, we reported the growth of single crystal NSOH NBs by a hydrothermal method. Sensitive humidity sensor was then fabricated with the nanobelts coated on ceramic substrate with Au interdigital electrodes. By measuring resistance of the device at different humidities and temperatures, the humidity sensing properties were studied. Resistance of the humidity sensor decreased monotonically with increasing RH. At 20 ℃, the resistance changes of more than four orders of magnitude was observed when NSOH NBs device was measured in 15% and 90% RH, respectively. The real-time response of the device show its rapid response and recovery time less than 3 s. Three months later, the measurement results show little variation. High sensitivity, fast response, long-term stability of the nanobelt sensor is potentially useful for humidity sensing. The high performance of the humidity sensor can to be contributed to its 1D morphology and its chemical composition.

Acknowledgements

This study was supported by the National Natural Science Foundation of China (Grant No. 21003041, 61376073), Hunan Provincial Natural Science Foundation of China (Grant No. 11JJ7004), and the Specialized Research Fund for the Doctoral Program of Higher Education of China (20120161110016)

Notes and references

1.College of electrical and information engineerin. Hunan University. Fax: +86 731 88664019; Tel: +86 731 88664019;
2.Key Laboratory for Micro-Nano Optoelectronic Devices of Ministry of Education Hunan University. State Key Laboratory for Chemo/Biosensing and Chemometrics Hunan University. Fax: +86 731 88822332; Tel: +86 731 88822332;
[a]E-mail: liqiuhong2004@hotmail.com [b]E-mail: thwang@iphy.ac.cn

† Electronic Supplementary Information (ESI) available: [details of any supplementary information available should be included here]. See DOI: 10.1039/b000000x/

‡ Footnotes should appear here. These might include comments relevant to but not central to the matter under discussion, limited experimental and spectral data, and crystallographic data.

1. G. Delapierre, H. Grange, B. Chambaz, L. Destaunes, *Sens. Actuators B* 1983 (4) 97~104.
2. G. Wang, Q. Wang, W. Lu and J. H. Li, *J. Phys. Chem. B* 2006 (110) 22029~22034.
3. Q. Kuang, C. S. Lao, Z. L. Wang, Z. X. Xie, L. S. Zheng, *J. Am. Chem. Soc.* 2007 (129) 6070-6071.
4. H. B. Hu, Q. W. Chen, K. C, J. Tang *J. Mater. Chem.*, 2012 (22) 1021~1027
5. Y. Zhu, J. C. Chen, H. M Li, Y. H. Zhu, J. Q. Xu *Sens. Actuators B* 2014 (193) 320~325
6. S. P. Chang, S. J. Chang, C. Y. Lu, M. J. Li, C. L. Hsu, Y. Z .Chiou, T. J. Hsueh, I. C. Chen, *Superlattices and Microstructures* 2010 (47) 772-778.
7. Y. S. Zhang, K. Yu, S. X. Ouyang, L. Q. Luo, H. M. Hu, Q. X. Zhang, Z. Q. Zhu, *physica B* 2005 (368) 94-99.
8. J. Xu, W. X. Zhang, Z. H. Yang, S. X. Ding, C. Y. Zeng, L. L. Chen, Q. Wang, S. H. Yang, *Adv. Funct. Mater.* 2009 *(*19) 1759-1766.
9. F. S. Tsai, S. J. Wang *Sens. Actuators B* 2014 (193) 280~287
10. J. D. Li, T. Fu, Y. J. Chen, B. K. Guan, M. Zhuo, T. Yang, Z. Xu, Q. L. Li, M. Zhang *CrystEngComm* 2014, accepted DOI:10.1039/C3CE42172D
11. Y. Cui, Q. Q. Wei, H. K. Park, C. M. Lieber, *Science* 2001 (293) 1289-1292.
12. A. Kolmakov, D. O. Klenov , Y. Lilach, S. Stemmer, and M. Moskovits, *Nano. Lett*. 2005 5667–673
13. Y. J. Chen, L. Nie, X. Y. Xue, Y. G. Wang, T. H. Wang, *appl. Phys. Lett.* 2006 (88) 083105
14. C. H. Kim, Y. Myung, Y. J. Cho, H. S. Kim, S. H. Park, J. Park, *J. Phys. Chem. C* 2009 (113) 7085-7090.
15. W. Kim, A. Javey, O. Vermesh, Q. Wang, Y. L, H. J. D, *nanolett.* 2003 (3) 193-198
16. A. Erol, S. Okur, N.Yaˇ gmurcukardes, M.C. Arıkan, *Sens. Actuators B* 2011 (152) 115~120
17. Y. Lu, Z. Y. Wang, S. Yuan, L. Y. Shi, Y. Zhao, W.Deng *RSC Adv.* 2013 (3) 11707-11714
18. U. Mogera, A. A. Sagade, S. J. George, G. U. Kulkarni *Sci. Rep.*2014 (4) 4103
19. L. L. Gu, K. B Zheng, Y. Zhou, J. Li, X. L. Mo, G. R. Patzkeb, G. R. Chen, *Sens. Actuators B* 2011 1591-7
20. M. H. Cao, X. Y. He, J. Chen, C. W. Hu *crystal growth design* 2007 (7) 170~174
21. D. E. Reisner, A. J. Salkind, P. R. Strutt, T. D. Xiao *Journal of power sources* 1997 (65) 231~233
22. M. B. J. G. Freitas *Journal of Power Sources* 2001 (93) 163~173
23. M. A. Kiani, M. F. Mousavi, S. Ghasemi *Journal of Power Sources* 2010 (195) 5794~5800
24. W. Wen, J. M. Wu, L. L. Lai, G. P. Ling, M. H. Cao, *CrystEngComm*. 2012 (14) 6565~6572
25. D. G. Yang, P. C. L, Y. Gao, H. Wu, Y. Cao, Q. Z. Xiao, H. M. Li, *J. Mater. Chem*. 2012 (22) 7224
26. L. Li, J. Liang, M. Luo, J. Z. Fang, *Powder Technology* 2012 (226) 143~146
27. H. Zhou, B. L. Lv, D. Wu, Y. H. Sun, *J Alloy. And Comp.* 2012 (540) 127~132
28. Z. Y. Jia IEEE 2011 673~677
29. K. Zhang, J. B. Wang, X. L. Lu, L. Y. Li, Y. W. Tang, Z. Y. J *J. Phys. Chem. C*. 2009 (113) 142~147
30. H. T. Hsueha, T.J. Hsueh, S. J. Chang, F. Y. Hung, T. Y. Tsai, W. Y. Weng, C. L. Hsu, B. T. Dai, *Sens. Actuators B* 2011 (156) 906-911
31. Y. S. Zhang, K. Yu, D. S. Jiang, Z. Q. Zhu, H. R. Geng, L. Q. Luo, *Applied surface science* 2005 (242) 212~217
32. S. Thakur, P. Patil *Sens. Actuators B* 2014 (194) 260~268
33. X. Q. Fu, C. Wang, H. C. Yu, Y. G. Wang, T. H. Wang, *Nanotechnology* 2007 (18) 145503
34. M. Trigo-López, A. Muñoz, S. Ibeas, F. C. García, F. Serna, J. M. García *Sens. Actuators B* 2014 (191) 233~238
35. G. Rubasinghege, V. H. Grassian *Chem. Commun.* 2013 (49) 3071~3094
36. C. L. Cao, C. G. Hu, L. Fang, S. X.Wang, Y. S. Tian, C. Y. Pan, *Journal of Nanomaterials* 2011 707303
37. J. H. Andersonl, G. A. Parks, *The Journal of Physical Chemistry* 1968 (72) 3662~3668
38. M. Zhuo, Y. Chen, J. Sun, H. Zhang, D. Guo, H. Zhang, Q. H. Li, T. H. Wang, Q. Wan *Sens. Actuators B* 2013 (186) 78~83.
39. Y. P. Zhang, J. Wu, Y. Zhang, W. B. Guo, S. P. Ruan *Sens. Actuators B* 2014 (14) 4303~4307
40. W. Van Gaens, A. Bogaerts *J. Phys. D: Appl. Phys*. 2014 (47) 079502 (3pp)